International Journal of Hybrid Information Technology
Vol. 9, No.11 (2016), pp. 323-336
http://dx.doi.org/10.14257/ijhit.2016.9.11.28

Bio-inspired Micro Pump Model Based on the Movement Pattern of Sperm

Feifei Liu[1], Xiaofei Ren[1+], Shoushui Wei[1]*and Zhiping Liu[1]

[1]*School of Control Science and Engineering, Shandong University, Jinan, Shandong 250061, China*
The first two authors contributed equally to this paper
**Corresponding author: Tel.: +86-13964062926, E-mail: sswei@sdu.edu.cn*

Abstract

Micro pumps play important roles in microfluidic system. Biologically inspired actuation mechanisms have great advantages in the micro pump design. This work aims to develop a numerical model for bio-inspired micro pump based on the specific and genuine –movement pattern of the sperm. The model also employs a modified immersed boundary-lattice Boltzmann method. In the model, an elastic film is used to mimic a sperm moving with its head fixed. The fluctuation vibration of the film could then drive the static fluid to move. The modified immersed boundary-lattice Boltzmann method directly introduces the velocity information of the film into the traditional lattice Boltzmann equation, which improve the computational efficiency. Pressure distribution, streamlines and the flow rate curves are used to analyze the flow field dynamic process of the model. The effects of the model parameters (e.g. frequency, kinematic viscosity, amplitude and wavelength) on the stable flow rate are also studied comprehensively.

Keywords*: Bio-inspired micro pump; Sperm; Flow field analysis; Parameter effect*

1. Introduction

Microfluidic systems have provided attractive solutions for many applications, such as drug delivery [1] , lab-on-a-chip [2], biological diagnostics [3] and food quality analysis [4]. Micro pumps, as the core component of microfluidic system, are essentially important but are often limited due to the factors of size, weight and cost [5]. Some novel micro pumps have been designed and studied [6]. They are mainly based on thermo-pneumatic [7], electrostatic [8], magnetic [9], electrodynamic [10] or piezoelectric [11] driving principles. In thermo-pneumatic micro pumps [7], large driving force could be achieved, but at the cost of high power consumption and slow response time. Conversely, electrostatic micro pumps [8] allow low power consumption and fast response time, whereas only small driving force could be achieved. Magnetic micro pumps [9] could offer both large driving force and fast response time, but they suffer from high power consumption and requirement of an external magnet. In addition, the electrodynamic micro pumps [10] are not suitable for the applications sensitive to electric fields. Many of new principles in flow pumps development are based on using piezoelectric actuators with simple structure, high output power density, precise metering capability, small power consumption and the ability of system integration.

Recently, bio-inspired propulsion mechanisms [12-14] based on the oscillating bimorph piezoelectric actuator [15, 16], such as flagella propulsion of a microorganism, has attracted widespread attention from academia and industry due to their advantages in simple structure, low fabrication cost and better controllability. Many researchers have designed the micro robot by the motion principle of microorganism [17, 18]. Sperm, with the length of a few hundred micrometers, reaches a speed of a few hundred microns per

ISSN: 1738-9968 IJHIT
Copyright © 2016 SERSC

second by propagating fluctuation down its tail [19]. However, if one held its head, when it tries to move, a fluid motion can be observed. These specific and genuine movement patterns transferred into fluid can be a viable option for innovative method of micro pumping with high performance. To this end, this work proposes a novel bio-inspired micro pump by using an elastic undulatory film with one fixed end to mimic the sperm movement.

For fluid-structure interaction of bio-inspired micro pump, Tabak *et al*. [20] and Lima *et al*. [21] studied the parameter influences of microfluidic by the finite element [22] and the finite difference [23] methods, respectively. However, these methods are inadaptable for the microscopic interactions [24]. In addition, such an approach has difficulties of mesh reconstruction in coupling nonlinear solid motions and fluid flow [25]. To solve this problem, lattice-Boltzmann method (LBM) [26] was proposed to achieve better results based on a 'semi-continuum' model with a mesoscopic kinetic equation for the particle distribution [27]. When dealing with the moving complex geometries problems, immersed boundary method (IBM) [28] considers the boundary as force source, and distributes it into lattice Boltzmann equation as a body force. This strategy avoids the difficulty of grid regeneration [29]. The combination of IBM and LBM (IB-LBM) has a variety of applications [30-32] for its certain advantages, such as high numerical efficient, easy handing of fluid-structure interaction, parallel algorithms.

IB-LBM was widely used to study the motion of the object in flowing fluid. However, in the inverse problem that the moving object drives the fluid to flow, IB-LBM needs to transform the structure variation of moving object into the deformation force to include the tension and bending forces. Therefore, the whole procedure of IB-LBM becomes tedious and the computational cost is high. Thus the modification in IB-LBM is needed for the bio-inspired micro pump.

Since the information of the film deformation including displacement, curve and length produced by the fluctuation velocity is easy to be obtained given the wave equations, the procedure of directly introducing the velocity information of the film into the lattice Boltzmann equation can avoid the complicated calculation of the deformation force. Therefore, we proposed an modified immersed boundary-lattice Boltzmann method (modified IB-LBM method) [33]. The modified IB-LBM method introduced immersed boundary into lattice Boltzmann equation as velocity source, which can avoid the transformation and significantly simplify the procedure.

In the work, we build a novel bio-inspired model for micro pump based on the movement pattern of the sperm by our previously proposed modified IB-LBM method. We analyze the flow filed and the parameter properties (including frequency, kinematic viscosity, amplitude and wavelength) of the novel micro pump. The study also finds that the sperm movement pattern can get the more flow rate. The modified IB-LBM method greatly improves the computational efficiency.

2. Methods

2.1. Model Design

As shown in Figure 1, a micro-tube model is designed as a rectangular area and is filled with viscous incompressible static fluid with the density of 1000kg/m^3. There is an infinite width of the flexible elastic film and the parallel plates in the z-direction. A two-dimensional model is applied in the simulated system. Since the two dimensional mode could catch the main fluid field characteristics. In addition, it can short the computing time. Tube wall is simulated by two parallel plates (200μm length) with a distance of 100μm.

The fluid domain is represented by Ω. In the $x-y$ reference frame, x is the horizontal coordinate of fluid domain (0-200μm from left to right), and y is the vertical coordinate of

 Copyright © 2016 SERSC

fluid domain (0-100μm from bottom to top). A flexible elastic film is horizontally placed near the bottom tube wall to act as the power source. The film has a length of 100μm and a thickness of 1μm. The film is not placed in the centre of the tube since the different flow characteristics between the left (Inlet) and right (Outlet) boundaries are expected to be observed. In addition, for easy to fabrication, the film is placed near the tube wall with a vertical distance of D_y. The distance D_x between the far left of film and the far left of tube wall is 10μm. The distance D_y between the film and the bottom tube wall is 10μm.

The inset of Figure 1 shows the combination of a bimorph [11]. The bimorph piezoelectric actuator is an electromechanical flexible actuator assembled as a clamped beam with a free end. The purple rectangles are piezoelectric material layers. The fixed end of the film is allocated between the piezoelectric material layers. When an electric voltage is applied to the piezoelectric material electrodes, the piezoelectric material with large shear modes are capable of causing large bending deformations, which can travel on the elastic film.

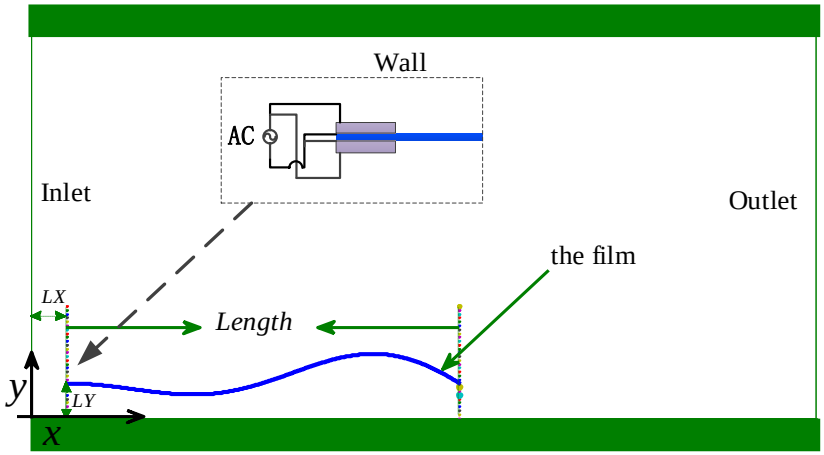

Figure 1. The Proposed Model of the Bio-Inspired Micro Pump. The Flexible Elastic Film (Blue Curve) With the Left End Fixed was Placed near the Bottom Tube Wall (Green Bold Line). The Left and Right Boundaries Are The Inlet and Outlet of the Micro-Tube Respectively. The Inset Shows the Combination of A Bimorph Which Drives the Film To Wave. The Purple Rectangles Are Piezoelectric Material Layers

2.2. Flow Field Simulation Using the Modified IB-LBM Method

The fluid in the rectangular area is initially as a static state and will be driven by the motion of the film. To generate the special motion mode, the left side of film is firstly fixed and then the film is driven to make a fluctuation with weighted amplitude. It is similar to the motion of sperm with the head fixed. The fluctuation is determined by the following formula

$$y_f(x_f,t)=\frac{x_f}{100}\times A\times\sin(2\pi ft-\frac{2\pi}{\lambda}x_f),\qquad x_f=0,1,\mathrm{L}\ 100 \tag{1}$$

where x_f is the horizontal coordinate of the film (0-100μm from left end to right end), A ,λ and f are the amplitude, wavelength and frequency of the fluctuation respectively. The position of flexible elastic film is denoted by $\boldsymbol{X}(x_f+\mathrm{D}_x,\ y_f+\mathrm{D}_y)$ in the fluid domain Ω.

Copyright © 2016 SERSC

Then the flow field is driven by the film fluctuation. The modified IB-LBM method regards the flexible elastic film as the velocity source because the information about film position and structure is all included in the film fluctuation velocity. The modified IB-LBM method could be described as follows

$$\Delta \boldsymbol{u}(\boldsymbol{n},t)=\int_0^{100}\frac{\partial \boldsymbol{X}(x_f+\mathrm{D}_x,y_f+\mathrm{D}_y)}{\partial t}\delta(\boldsymbol{n}-\boldsymbol{X}(x_f+\mathrm{D}_x,y_f+\mathrm{D}_y))\mathrm{d}x_f \tag{2}$$

$$\boldsymbol{u}(\boldsymbol{n},t+1)=\frac{\sum_i \boldsymbol{e}_i f_{\mathrm{i}}^{eq}(\boldsymbol{n},t)}{\sum_i f_i^{eq}(\boldsymbol{n},t)}+\Delta \boldsymbol{u}(\boldsymbol{n},t) \tag{3}$$

where $\boldsymbol{u}(\boldsymbol{n},t)$ was the fluid velocity. The horizontal coordinate of fluid domain x is discretized into n_x with the step size 0.1μm. The vertical coordinate of fluid domain y is discretized into n_y with the step size 0.1μm. Two-dimensional vector $\boldsymbol{n}$, including n_x and n_y, is applied for the position of each fluid lattice. $\boldsymbol{X}(x_f+\mathrm{D}_x,y_f+\mathrm{D}_y)$ is the position of the flexible elastic film. $\frac{\partial \boldsymbol{X}(x_f+\mathrm{D}_x,y_f+\mathrm{D}_y)}{\partial t}$ is the velocity of flexible elastic film. $\delta(\boldsymbol{n}-\boldsymbol{X})$ is the Dirac delta function. $f_i^{eq}(\boldsymbol{x},t)$ is the local fluid density equilibrium distribution function.

The lattice model D2G9 of LBM [34] for two-dimensional simulations is applied. Sperm and other aquatic microorganisms are mostly living in the liquid environment. So the fluid with the density of 1000kg/m^3 is used in our simulation. Most of the existing lattice Boltzmann BGK models (LBGK) can be viewed as compressible schemes to simulate incompressible fluid flows. The compressible effect might lead to some undesirable errors in numerical simulations [35]. D2G9 is a LBGK model without compressible effect. The incompressible Navier–Stokes equations are exactly recovered from this incompressible LBGK model [36], which is more suitable for our simulation.

In the lattice model D2G9 of LBM, $i=0,1,\mathrm{L}\ ,8$ denotes the lattice direction and $\boldsymbol{e}_i$ is the lattice velocity. $f_i(\boldsymbol{n},\mathrm{t})$ is the fluid density distribution function, indicating the particle amount moving along the i lattice direction with velocity $\boldsymbol{e}_i$ at time t, with the form of

$$f_i(\boldsymbol{n}+\boldsymbol{e}_i\Delta t,t+\Delta t)=f_i(\boldsymbol{x},t)-\frac{1}{\tau}[f_i(\boldsymbol{x},t)-f_i^{eq}(\boldsymbol{x},t)], \tag{4}$$

where Δt is the time step. For the D2G9 model, the local fluid density equilibrium distribution function $f_i^{eq}(\boldsymbol{x},t)$ is given by

$$f_i^{eq}(\boldsymbol{x},t)=\begin{cases}\rho-\dfrac{5p}{3c^2}+\rho\omega_i[\dfrac{3\boldsymbol{u}\cdot\boldsymbol{e}_i}{c^2}+\dfrac{9}{2}(\dfrac{\boldsymbol{u}\cdot\boldsymbol{e}_i}{c^2})^2-\dfrac{3}{2}(\dfrac{\boldsymbol{u}^2}{c^2})] & i=0\\ \dfrac{p}{3c^2}+\rho\omega_i[\dfrac{3\boldsymbol{u}\cdot\boldsymbol{e}_i}{c^2}+\dfrac{9}{2}(\dfrac{\boldsymbol{u}\cdot\boldsymbol{e}_i}{c^2})^2-\dfrac{3}{2}(\dfrac{\boldsymbol{u}^2}{c^2})] & i=1,2,3,4\\ \dfrac{p}{12c^2}+\rho\omega_i[\dfrac{3\boldsymbol{u}\cdot\boldsymbol{e}_i}{c^2}+\dfrac{9}{2}(\dfrac{\boldsymbol{u}\cdot\boldsymbol{e}_i}{c^2})^2-\dfrac{3}{2}(\dfrac{\boldsymbol{u}^2}{c^2})] & i=5,6,7,8\end{cases} \tag{5}$$

where ρ is the density of the fluid, ω_i is the weighting factor for the various lattice links, $c=\frac{\Delta n}{\Delta t}$ is the particle streaming speed, Δn is lattice spacing. The pressure of fluid p is directly calculated from the distribution function by

$$p=\rho\frac{3c^2}{5}\left\{\sum_{i=1}^{8}f_i+\rho\omega_0[\frac{3\boldsymbol{u}\cdot\boldsymbol{e}_0}{c^2}+\frac{9}{2}(\frac{\boldsymbol{u}\cdot\boldsymbol{e}_0}{c^2})^2-\frac{3}{2}(\frac{\boldsymbol{u}^2}{c^2})]\right\}. \tag{6}$$

 Copyright © 2016 SERSC

For the D2G9 model, the weighting factor for the various lattice links ω_i and the discrete velocities of the fluid particles $\boldsymbol{e}_i$ are given by

$$\omega_i = \begin{cases} \frac{4}{9} & i = 0 \\ \frac{1}{36} & i = 1,2,3,4 \\ \frac{1}{9} & i = 5,6,7,8 \end{cases} \tag{7}$$

$$\boldsymbol{e}_i = \begin{cases} 0 & i = 0 \\ (\cos[\frac{\pi(i-1)}{2}], \sin[\frac{\pi(i-1)}{2}])c & i = 1,2,3,4 \\ \sqrt{2}(\cos[\frac{\pi(i-9/2)}{2}], \sin[\frac{\pi(i-9/2)}{2}])c & i = 5,6,7,8. \end{cases} \tag{8}$$

The relaxation time τ in Eq. (4) is directly related to the kinematic viscosity of the fluid v by the following equation

$$\tau = \frac{3v}{c^2 \Delta t} + \frac{1}{2}. \tag{9}$$

At the inlet and outlet, the non-equilibrium extrapolation scheme [37] is applied. Bounce back [38] method is used between the fluid and the walls to implement non-slip condition.

3. Results

According to the Eq. (1) - Eq. (6), the parameters of amplitude, frequency and wavelength of the fluctuation affected the fluid flow by determining the velocity information. In addition, the kinematic viscosity of fluid also played a major role on the fluid mechanics, which is related with the relaxation time τ in LBM equations. So the numerical-simulation experiments are carried out to test the effects of the flexible elastic film fluctuation deformations on pressure distribution, flow streamlines and instantaneous flow rate, and to comprehensively explore the parameter influences, like frequency, kinematic viscosity of the fluid, amplitude and wavelength.

3.1. Dynamic Process of the Flow Field

Figure 2 shows the pressure distributions (A1-A4) and flow streamlines (B1-B4) of the flow field at t = 0, 3, 30, and 300 cycles, since the constant flow rate is achieved after 300 cycles. High pressure (deep red) takes place on the side of the film pushing the fluid, while low pressure (deep blue) takes on the side pulling the fluid. High and low pressure regions are spread out and influenced by the rebound effect of the wall. The high (low) pressure increases its intensity gradually from the left fixed end to the right free end, which corresponds to weighted amplitude of the film. The simulation is run over 500 cycles of the film fluctuation with the specified parameters setting as shown in Table 1.

For the instantaneous streamlines of the flow field, there are no streamlines when t=0 cycle. When t=3, 30 cycles, streamlines spread outward from the film with the pressure gradient and produce a recirculation at the free end. There is no fixed pattern of streamlines until the system is steady. When t=300 cycles, the constant flow rate has been achieved. The streamlines of flow expand from the film to the wall of the tube and are influenced by rebound effect. The flow is uniform at the exit of the channel, but near the inlet, there is a strong recirculation.

Copyright © 2016 SERSC

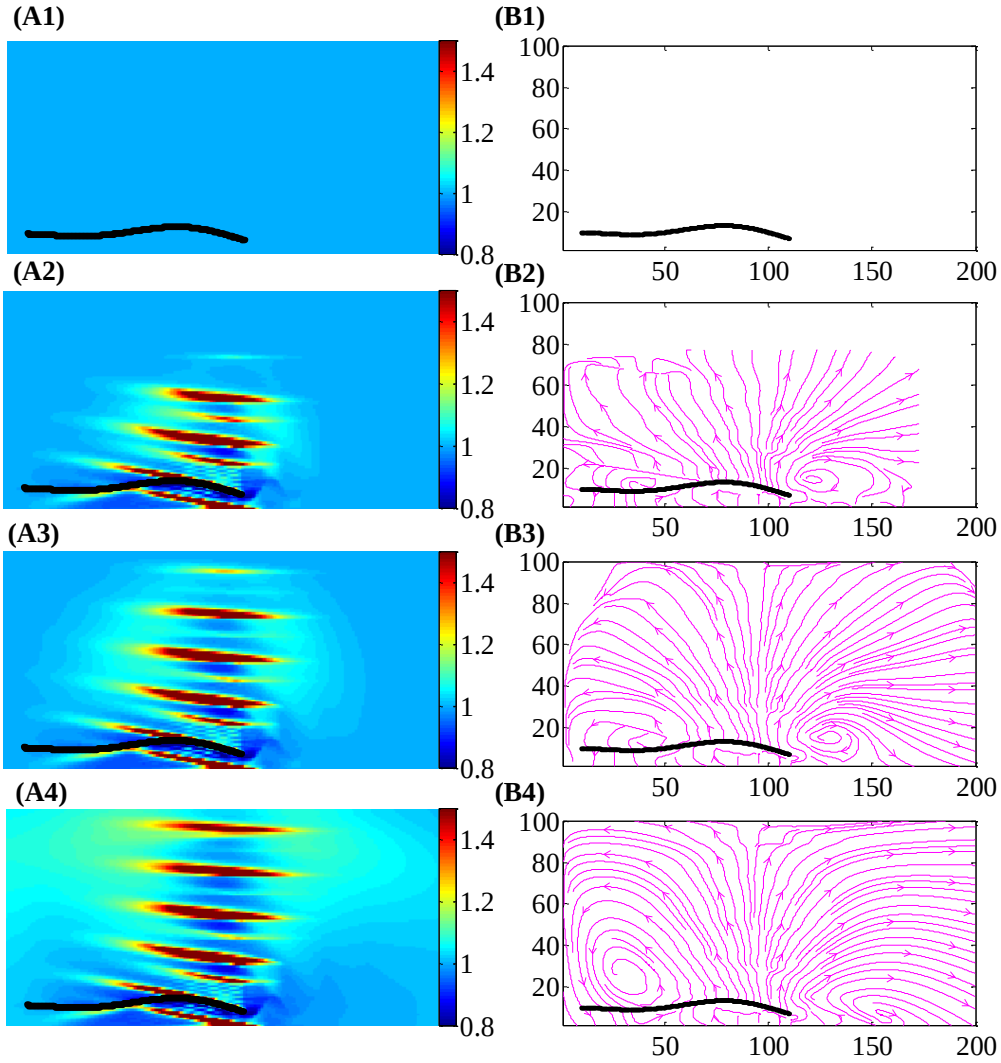

Figure 2. Snapshots of the Pressure Distribution (A1-A4) and Streamlines (B1-B4). These Snapshots are from the Time of t=0 Cycle (A1 and B1), t=3 Cycles (A2 and B2), t=30 Cycles (A3 and B3), t=300 Cycles (A4 and B4)

In order to view the film undulation, Figure 3 shows pressure distributions and flow streamlines in the flow field at t = 0.2, 3.4, 30.6, and 300.8 cycles. It is clear that the flexible elastic film moves like sperm with the head fixed and drives the fluid to flow. These high and low pressure couples move along the direction of the fluctuation propagation.

Copyright © 2016 SERSC

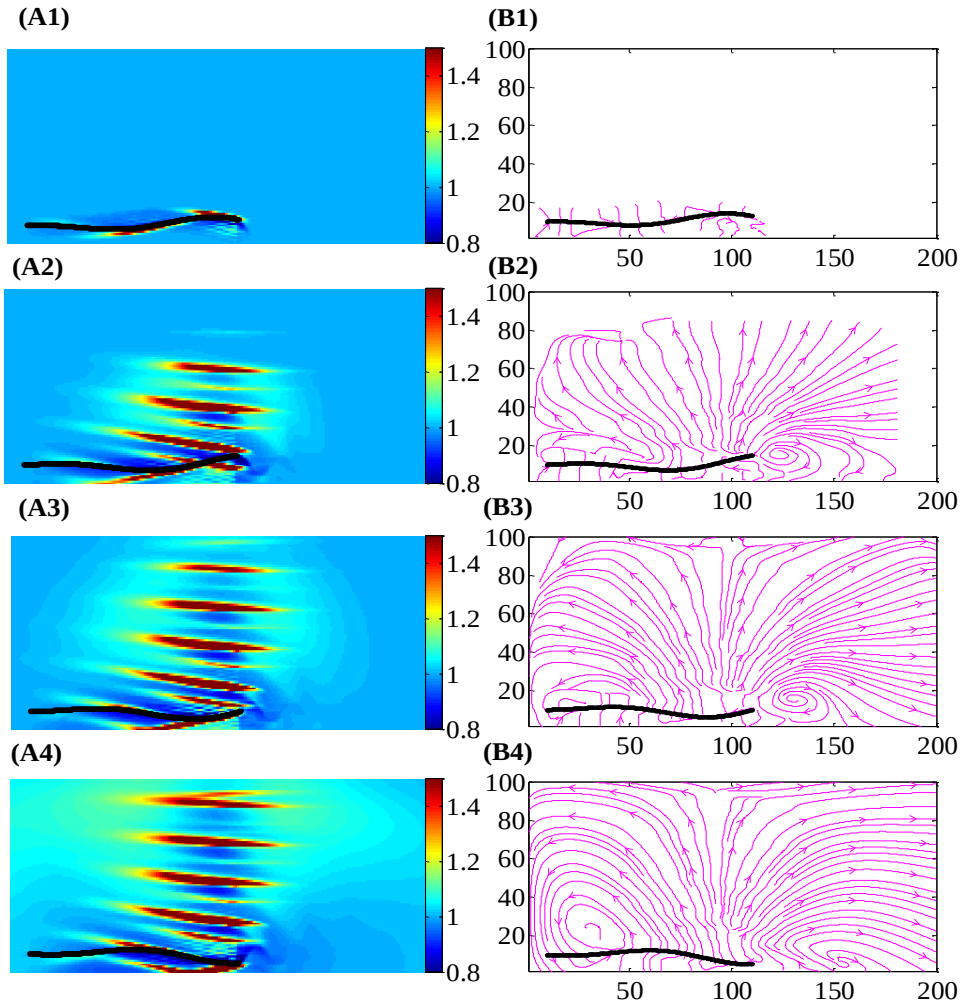

Figure 3. Snapshots of the Pressure Distribution (A1-A4) and Streamlines (B1-B4). These Snapshots are from the Time of *t*=0.2 Cycles (A1 and B1), *t*=3.4 Cycles (A2 and B2), *t*=30.6 Cycles (A3 and B3), *t*=300.8 Cycles (A4 and B4). The Fluctuation of the film and the Resulting Changes in Pressure Distribution and Streamlines Could Be Observed by the Slight Time Changes Compared with Figure 2

Table 1. Default Settings for the Four Parameters

Parameters	Value
frequency (f)	5 [Hz]
kinematic viscosity of the fluid (v)	1.5×10^{-6} [$m^2 \cdot s^{-1}$]
wavelength (λ)	100 [μm]
amplitude (A)	5 [μm]

Copyright © 2016 SERSC

Figure 4 gives the instantaneous flow rate curve as a function of time. The specified parameter setting is shown in Table 1. After 300 cycles of the fluctuation, the flow rate is near constant. So we simulated over 500 cycles. The instantaneous mass flow rate is calculated by the integration of product of the *x*-component of the velocity and the density of fluid at the outlet

$$Q(t) = \sum_{n_y=0}^{100} u(\boldsymbol{n}(200, n_y), t) \times \rho(\boldsymbol{n}(200, n_y), t), \tag{10}$$

where $u(\boldsymbol{n}(200,\ n_y), t)$ and $\rho(\boldsymbol{n}(200, n_y), t)$ are the x -component of the velocity and the density at the position $(200, n_y)$ at time t.

In Figure 4, as blue solid line shown, the mass flow rate is zero at the beginning. Then, it increases quickly. At last, it slows down and converges to a constant flow rate value, 0.43μg·min^{-1}·μm^{-2}, which is the stable flow rate Q. At this time, the pump has reached a stationary state. The red dashed line is the standard line for Q =0.43μg·min^{-1}·μm^{-2}.

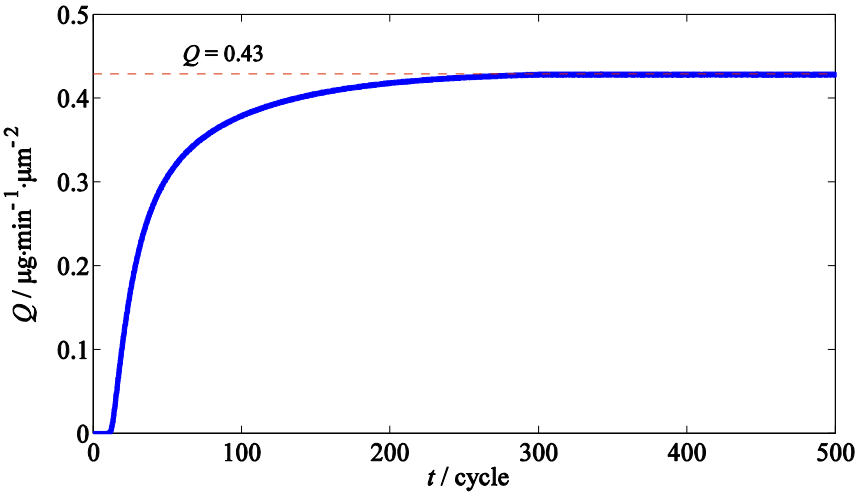

Figure 4. The Flow Rate *Q* (*t*) as a Function of Time

3.2. Influence of the Fluctuation Form

In the references [20, 33], the fluctuating film micro pump were studied. However, the fluctuation form was different from that of our paper. In these references, the film vibrated with two fixed ends. So we designed another model as Figure 1 except that the right end of the film was fixed. This fluctuation is different from the motion of sperm. Table 2 lists the flow rates between this two different fluctuation form under the same equipment and parameter setting for the scale parameter k ($k = 0.1, 1$ and 2). When $k = 1$, the parameters are equal to the default values in Table 1. As shown in Table 2, the flow rate of the bio-inspired fluctuation is larger than that of vibrating film with two fixed ends.

Table 2. Comparisons of the Stable Flow rate for Different Fluctuation Form

Fluctuation form	k = 0.1	k = 1	k = 2
	Q /μg·min^{-1}·μm^{-2}	Q /μg·min^{-1}·μm^{-2}	Q /μg·min^{-1}·μm^{-2}
fluctuating film with two fixed ends	0.0004	0.022	1.05
Bio-inspired fluctuating film	**0.003**	**0.43**	**12.1**

Copyright © 2016 SERSC

3.3. Effects of Parameter Change on the Stable Flow Rate *Q*

Figure 5 shows the stable flow rate Q as a function of the scale parameter k ($k = 0.1, 0.2 \text{ L L } 1.8, 1.9, 2$) for different parameters. One parameter varies directly in multiples of k while other parameters are the default values in Table 1. In the case of frequency, its range is from 0.5Hz to 10Hz and the step size is 0.5Hz. As shown, when k=1, four curves intersect in a single point. Apparently, different parameters have different influences on the stable mass flow rate Q. The effect of varying wavelength is slighter than those of other parameters.

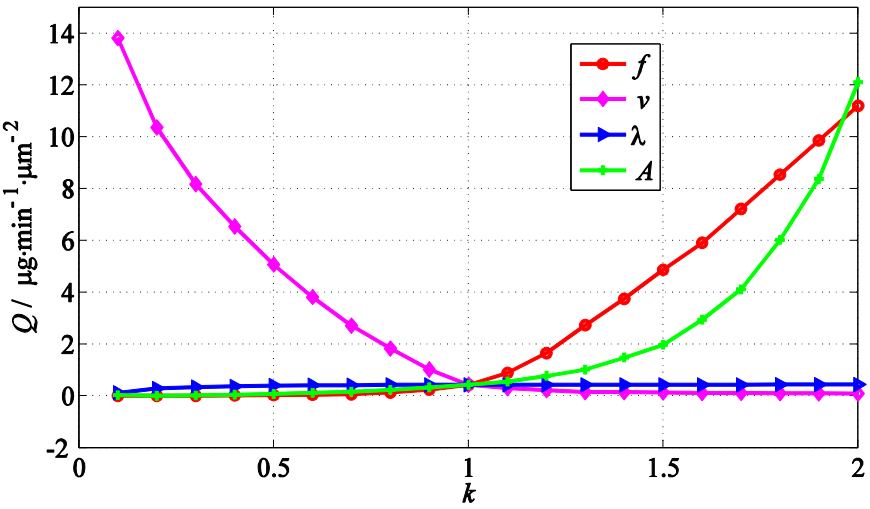

Figure 5. The Changes of Stable Flow Rate *Q* with the Changes of Four Parameters (Frequency, Kinematic Viscosity, Amplitude and Wavelength) At Different Scale Parameter *K* Levels

In Figure 5, the red circle solid line gives the cubic increasing relationship between the stable flow rate Q and varying frequency f; the pink rhombus solid line represents the negative exponential function between the stable flow rate Q and the kinematic viscosity of fluid v; the green cross solid line shows the stable flow rate increases with six power of amplitude A; the blue triangle solid line plots the stable flow rate Q as a function of varying wavelength λ. Combining effects of four parameters, a flow rate coefficient is defined as follows

$$P_Q = \mathrm{C}_1(A^6 + \mathrm{C}_2) f^3 e^{-\frac{9}{5}v}(-\frac{4}{\lambda} + \mathrm{C}_3). \tag{11}$$

where $\mathrm{C}_1, \mathrm{C}_2$ and C_3 are constant. In this mode, $\mathrm{C}_1 = 4.4 \times 10^{-7}$, $\mathrm{C}_2 = 48$, $\mathrm{C}_3 = 0.45$.

3.4. Comparison of the Computational Efficiency

Table 3 lists the running times and the stable flow rates of software, COMSOL Multiphysics [39], the conventional IB-LBM and the modified IB-LBM method for $k = 0.1, 1$ and 2 under the same equipment and parameter setting. As shown in Table 3, compared with the other two methods, the modified IB-LBM method obtained better results. When using IB-LBM and COMSOL Multiphysics, the running time is about twice as much as that of the modified IB-LBM method.

Copyright © 2016 SERSC

Table 3. Comparisons of the Stable Flow Rate (*Q*) and Running Time

Methods	k = 0.1		k = 1		k = 2	
	Q /μg·min^{-1}·μm^{-2}	time /s	Q /μg·min^{-1}·μm^{-2}	time /s	Q /μg·min^{-1}·μm^{-2}	time /s
Finite-difference method	0.003	1024	0.42	1521	12.5	2603
IB-LBM	0.002	1362	0.40	2015	12.0	2985
Modified IB-LBM method	0.003	**530**	0.43	**768**	12.1	**1222**

4. Discussion

Based on the modified IB-LBM method, we developed a novel numerical model for bio-inspired micro pump to explore the parameter influences of the fluctuation with the genuine pattern of sperm movement on the flow field. The fluctuation was generated on an elastic film to mimic sperm moving with its head fixed. As the film waved, the film yielded thrust force and pull force to drive the fluid to move. It is worth to note that the high and low pressure regions appeared and spread out, where net pressure difference produced a net stable flow rate at the outlet and a steady circulation near the inlet. The reason for the steady circulation is that the fluctuation amplitude of the film gradually increased from the left fixed end to the right free end. The influence of the film on the fluid gradually intensified from the fixed end to the free end, and hence a steady circulation is produced near the inlet, which can decrease the counter-flow at the inlet.

Compared with the fluctuation form with two fixed ends, bio-inspired fluctuation could get larger flow rate. Since the specific movement pattern of sperm can drive it to move with a speed of a few hundred microns per second, this movement pattern produces large acting force on the fluid.

The parameters are crucial for the controllability of flow. So we comprehensively explored the model parameter effects on the proposed bio-inspired micro pump. It has been shown that the increasing frequency and amplitude resulted in an increase of the stable flow rate. According to Eq. (1) - Eq. (3), the velocity of the film increased as the frequency and amplitude increased, which resulted in the power transferred into the fluid also increased. The increasing kinematic viscosity induced a quick decrease of the flow rate due to viscous damping of the surrounding fluid. The reason of the non-linear relationships between the stable flow rate and wavelength is because large curvature of the film could reduce driving efficiency, and the curvature can decrease as the wavelength increases.

A flow rate experimental formula $C_Q = \pi\sqrt{\lambda} fA^2/50$ was also given in reference [20]. It is noted that C_Q is different from the flow rate coefficient P_Q of the proposed paper. Figure 6 gives the stable mass flow rate *Q* as functions of varying frequency (A: red circle solid line), kinematic viscosity (B: pink rhombus solid line), wavelength (C: blue triangle solid line) and amplitude (D: green cross solid line) in detail, with one parameter varies directly in multiples of *k* while other parameters are the default values. For comparison, the black dashed lines in Figure. 6(A, C, D) show the relationship between the final stable flow rate and the frequency, wavelength and amplitude according to C_Q. The main reason of the difference is the film setting. The inextensible film with two fixed end was placed at the center of the tube in the reference [20], while the extensible film with one free end and one fixed end similarly to the sperm was placed near the left bottom. Another reason

 Copyright © 2016 SERSC

for difference is that the influence of the kinematic viscosity of fluid on the flow rate was not considered in the reference[20].

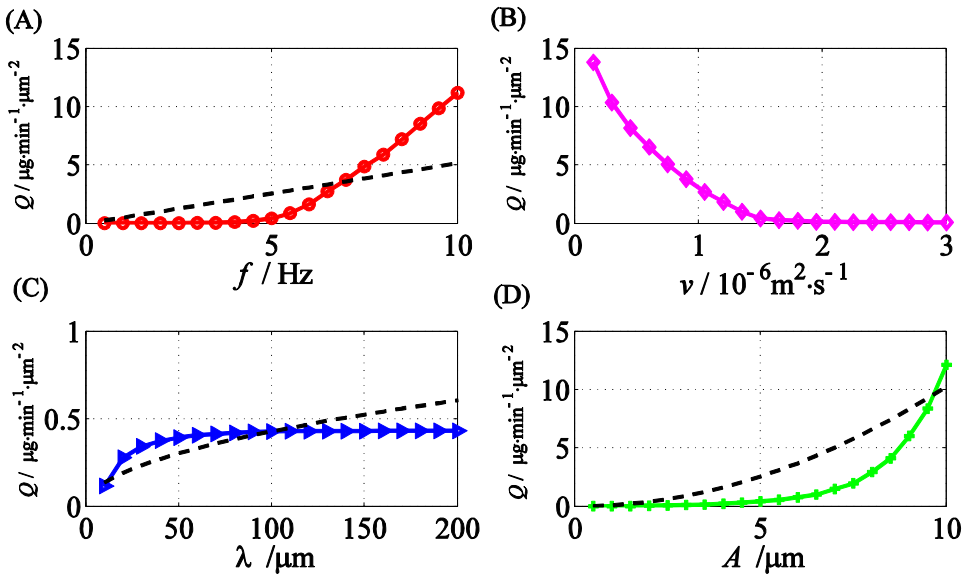

Figure 6. The Solid Lines Show the Relationships between the Stable Flow Rate *Q* and the Different Parameters: Frequency *F* (A), Kinematic Viscosity of the Fluid *V* (B), Wavelength *Λ* (C) and Amplitude *A* (D). The Black Dashed Lines Show the Simulated Results From Formula $C_Q = \pi\sqrt{\lambda} f A^2/50$

Compared with using COMSOL multiphysics and the traditional IB-LBM, the modified IB-LBM method had a better computational efficiency. The efficiency improvement is due to the velocity information including film shape deformation was directly introduced into the Lattice Boltzmann equation, which avoided the transformation among the fluctuation velocity, the film shape deformation and the force density.

5. Conclusion

We constructed a mesoscopic scale bio-inspired micro pump by the modified IB-LBM method. This work demonstrated that the modified IB-LBM method could provide a new insight for the design of micro pump that the moving object drove the viscous fluid to flow. We have also demonstrated that bio-inspired fluctuation form can get larger flow rate. The parameter setting is identified to be crucial for the bio-inspired micro pump. These findings are important for building model-based micro pumps, and they are very useful in promoting bionic microfluidic system development.

Acknowledgments

This study was partially supported by National Natural Science Foundation of China (Grant No. 51075243, 11002083), and the Natural Science Foundation of Shandong Province (Grant No. ZR2014EEM003, ZR2014AM031)

Copyright © 2016 SERSC

References

[1] Q.B. Xu, M. Hashimoto, T.T. Dang, T. Hoare, D.S. Kohane, G.M. Whitesides, R. Langer and D.G. Anderson, Small, vol. 13, no. 5, **(2009)**.
[2] C. Huang and C. Tsou, Sensor Actuat A-Phys, vol. 210, no. 6, **(2014)**.
[3] J.M. Huttunen, H.T. Kokkonen, J.S. Jurvelin, J. Töyräs and J.P. Kaipio, Int J Numer Meth Eng, vol. 98, no. 67, **(2014)**.
[4] H. Komatsuzaki, K. Suzuki, Y. Liu, T. Kosugi, R. Ikoma, S.-W. Youn, M. Takahashi, R. Maeda and Y. Nishioka, Jpn J Appl Phys, vol. 6, no. 50, **(2011)**.
[5] M.L. Cantwell, F. Amirouche and J. Citerin, Sensor Actuat A-Phys, vol. 1, no. 168, **(2011)**.
[6] B.D. Iverson and S.V. Garimella, Microfluid Nanofluid, vol. 2, no. 5, **(2008)**.
[7] Y.C. Ou, C.S. Yu, C.C. Yang, C.M. Chang, Y.H. Tang and Y.H. Lin, J Appl Sci Eng, vol. 4, no. 15, **(2012)**.
[8] F. Amirouche, Y. Zhou and T. Johnson, Microsyst technol, vol. 5, no. 15, **(2009)**.
[9] M. Shen, L. Dovat and M. Gijs, Sensor Actuat B-Chem, vol. 1, no. 154, **(2011)**.
[10] A. Homsy, S. Koster and J.C. Eijkel, Lab Chip, vol. 4, no. 5, **(2005)**.
[11] C.R. de Lima, S.L. Vatanabe, A. Choi, P.H. Nakasone, R.F. Pires and E.C.N. Silva, Sensor Actuat A-Phys, vol. 1, no. 152, **(2009)**.
[12] J.M. Li, C. Liu, Z. Xu, K.P. Zhang, X. Ke, C.Y. Li and L.D. Wang, Lab Chip, vol. 16, no. 11, **(2011)**.
[13] I.N. Vieira, B.S.L.P. Lima and B.P. Jacob, Int J Numer Meth Eng, vol. 10, no. 91, **(2012)**.
[14] C.Y. Yang, C.F. Chen, Q.F. Ma, L.F. Wu and T. Song, J Bionic Eng, vol. 2, no. 9, **(2012)**.
[15] M. Kogl and E.C.N. Silva, Smart Materials & Structures, vol. 2, no. 14, **(2005)**.
[16] E.C.N. Silva, J Intel Mat Syst Str, vol. 4, no. 14, **(2003)**.
[17] B. Chen, S. Jiang, Y. Liu, P. Yang and S. Chen, J Bionic Eng, vol. 7, **(2010)**.
[18] B. Chen, Y.D. Liu, S. Chen, S.r. Jiang and H.T. Wu, J Bionic Eng, vol. 5, **(2008)**.
[19] F.H. Qin, W.X. Huang and H.J. Sung, Comput Fluid, vol. 55, **(2012)**.
[20] A.F. Tabak and S. Yesilyurt, Microfluid Nanofluid, vol. 6, no. 4, **(2008)**.
[21] C.R. Lima, S.L. Vatanabe, A. Choi, P.H. Nakasone, R.F. Pires and E.C. Nelli Silva, Sensor Actuat A-Phys, vol. 1, no. 152, **(2009)**.
[22] T.N. Tran, G. Liu, H. Nguyen and T. Nguyen, Int J Numer Meth Eng, vol. 7, no. 82, **(2010)**.
[23] M. Cho and H. Kim, Int J Numer Meth Eng, vol. 1, no. 62, **(2005)**.
[24] J.F. Zhang, Microfluid Nanofluid, vol. 1, no. 10, **(2011)**.
[25] F. B. Tian, H. Luo, L. Zhu, J.C. Liao and X. Y. Lu, J comput phys, vol. 19, no. 230, **(2011)**.
[26] J. Zhang, G. Yan, X. Shi and D. Yinfeng, Int J Numer Meth Fluid, vol. 1, no. 60, **(2009)**.
[27] D.V. Patil and K.N. Lakshmisha, Int J Numer Meth Fluid, vol. 6, no. 69, **(2012)**.
[28] S.K. Kang and Y.A. Hassan, Int J Numer Meth Fluid, vol. 9, no. 66, **(2011)**.
[29] S. Yamasaki, T. Yamada and T. Matsumoto, Int J Numer Meth Eng, vol. 9, no. 93, **(2013)**.
[30] M. Navidbakhsh and M. Rezazadeh, Sci Iran, vol. 5, no. 19, **(2012)**.
[31] X.W. Yin, T. Thomas and J.F. Zhang, Microvasc Res, vol. 89, **(2013)**.
[32] R. Cortez, L. Fauci, N. Cowen, R. Dillon, Comput Sci Eng, 3, 6 (**2004**).
[33] F.F. Liu, S.S. Wei, S.W. Wang, C.Z. Wei and X.F. Ren, J Nanoengin. Nanosys., vol. 4, no. 228, **(2014)**.
[34] Y.Y. Yan, Y.Q. Zu and B.O. Dong, Appl Therm Eng, vol. 5, no. 31, **(2011)**.
[35] Z. Guo, B. Shi and N. Wang, J Comput Phys, vol. 1, no. 165, **(2000)**.
[36] Z.L. Guo, B.C. Shi and C.G. Zheng, Int J Numer Meth Fluid, vol. 4, no. 39, **(2002)**.
[37] J.Y. Shao, C. Shu, J. Wu and Y.T. Chew, Inte J Numer Meth Fluid, vol. 6, no. 72, **(2013)**.
[38] [38] S. Krithivasan, S. Wahal and S. Ansumali, Phys Rev E, vol. 3, no. 89, **(2014)**.
[39] E.J.F. Dickinson, H. Ekstrom and E. Fontes, Electrochem Commun, vol. 40, no. 87, **(2014)**.

 Copyright © 2016 SERSC

Authors

Feifei Liu, she was born in Jinan, China, September 1987. In 2015, she received PhD degree from Shandong University. Currently, she is a Lecturer at Shandong Jiaotong University. Her research interests include microfluidic driving and control.

Shoushui Wei, he is a Professor in Shandong University. His research interests include microfluidic driving and control, biomedical signal processing.

Copyright © 2016 SERSC

 Copyright © 2016 SERSC